Ahmed Ghorbel*, Walid Aydi, Imen Tajouri and Nouri Masmoudi

Hybrid Approach for Face Recognition from a Single Sample per Person by Combining VLC and GOM

https://doi.org/10.1515/jisys-2018-0380
Received September 17, 2018; previously published online August 14, 2019.

Abstract: This paper proposes a new face recognition system based on combining two feature extraction techniques: the Vander Lugt correlator (VLC) and Gabor ordinal measures (GOM). The proposed system relies on the execution speed of VLC and the robustness of GOM. In this system, we applied the Tan and Triggs and retina modeling enhancement techniques, which are well suited for VLC and GOM, respectively. We evaluated our system on the standard FERET probe data sets and on extended YaleB database. The obtained results exhibited better face recognition rates in a shorter execution time compared to the GOM technique.

Keywords: Face recognition, VLC, GOM.

1 Introduction

Because of the increase and complexity of criminal behavior in modern societies, robust and efficient authentication systems became vital. Compared to traditional token (Id Card, badge, …) and knowledge-based systems (PIN, Password, …), which can be either forgotten or stolen, biometric authentication systems offer a better solution for a wide range of applications like access control, criminal identification, etc.

Different modalities are used in biometric systems such as iris, fingerprint, voice, and face recognition. The latter is widely used for many factors. Interestingly, such a system is able to recognize people without their interaction. In addition, this makes the task more difficult due to some challenging factors such as pose variation, luminosity, facial expression in addition to the aging and the time-precision compromise. A face recognition system rests on four main steps: face detection, preprocessing, feature extraction, and classification.

The Gabor wavelet feature extraction techniques showed promising results in face recognition applications like the Gabor ordinal measures (GOM) [4, 9] and optic-based techniques like the Vander Lugt correlator (VLC) [1, 8], which represents a fast face recognition system.

In this paper, we propose combining these two techniques in order to take profit from the speed of VLC and the precision of GOM.

This work is outlined as follows: in Section 2, we describe the preprocessing techniques used in our system. Section 3 contains our proposed hybrid face recognition system. The experimental results are presented in Section 4. Finally, conclusions are drawn in Section 5.

***Corresponding author: Ahmed Ghorbel,** Laboratory of Electronics and Information Technologies, University of Sfax, Sfax, Tunisia, e-mail: ghorbelahmed@ymail.com
Walid Aydi: Laboratory of Electronics and Information Technologies, University of Sfax, Sfax, Tunisia; and College of Sciences and Humanities – Aflaj, Prince Sattam bin Abdulaziz University, Al-Kharj, Saudi Arabia
Imen Tajouri and Nouri Masmoudi: Laboratory of Electronics and Information Technologies, University of Sfax, Sfax, Tunisia

2 Preprocessing

Preprocessing is a crucial step for feature extraction and then for the performance of the face recognition system. This preprocessing is composed of three steps as shown in Figure 1: landmark detection, image alignment and cropping, and Tan and Triggs [20, 21] preprocessing or retina modeling.

2.1 Landmark Detection

In general, there are three main methods to locate the facial landmarks from a face image: the first category performs a sliding window search based on local-patch classifiers, which encounters the problems of the ambiguity or corruption in local features [25]. The second category of methods is the well-known framework of the active shape model (ASM) [2] and the active appearance model (AAM) [5]. These methods fit a generative model for the global facial appearance and are, hence, robust to local corruptions. However, to estimate the parameters in the generative models, expensive iterative steps are required.

Recently, a new framework based on explicit regression methods was proposed [3, 18]. In this framework, the problem of landmark localization is considered directly as a regression task, and a holistic regression is used to compute the landmark coordinates from raw input pixels. Compared to the previous methods, this framework is more robust and stable as the global contextual information is incorporated at the beginning. It is also more efficient as no iterative fitting step or sliding window search is required. Instead of the random ferns (group of features) used in Ref. [3], Sun et al. [18] applied a more powerful deep convolutional neural network (DCNN) in the regression framework and achieved a state-of-the-art performance [25].

2.2 Tan and Triggs

The preprocessing technique proposed by Tan and Triggs consists of three steps [21]: gamma correction, Difference of Gaussian (DoG) filtering, and contrast equalization as shown in the Figure 2.

2.2.1 Gamma Correction

The gamma correction is a nonlinear gray-level transformation that replaces the gray-level I with I_{GC}

$$I_{GC} = \begin{cases} I^{\gamma} & \text{if } \gamma > 0 \\ \log(I) & \text{if } \gamma = 0 \end{cases} \tag{1}$$

where $\gamma \in [0, 1]$ is a user-defined parameter. It has the effect of enhancing the local dynamic range of the image in dark or shadowed regions, while compressing it in bright and at highlight regions.

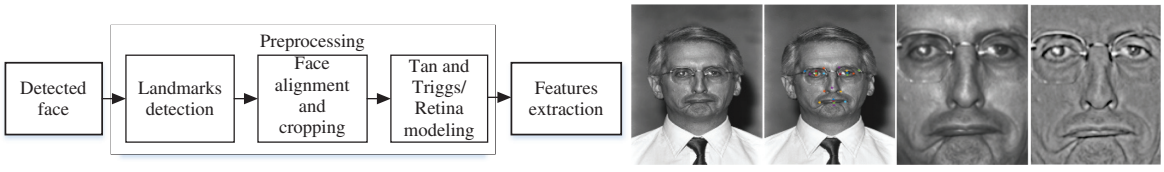

Figure 1: Preprocessing Step.

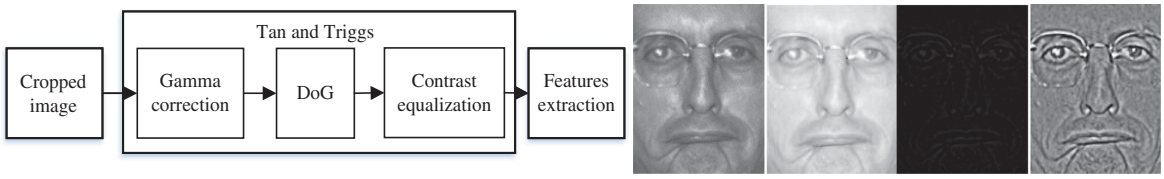

Figure 2: Tan and Triggs Preprocessing.

2.2.2 DoG Filtering

This step is achieved by a convolutional product between the enhanced image I' and the DoG filter. The DoG filter is a bandpass filter described by equation (2). The high-pass filtering simplifies the recognition by removing the incidental information and reducing the aliasing and noise without affecting the performance of the recognition system. Instead, in many cases, the high-pass filter increases the performance.

$$DoG(x,y) = \frac{1}{2\pi}\left[\frac{1}{\sigma_1^2}e^{-\frac{x^2+y^2}{\sigma_1^2}} - \frac{1}{\sigma_2^2}e^{-\frac{x^2+y^2}{\sigma_2^2}}\right] \tag{2}$$

where the standard deviations of the two Gaussians are $\sigma_1 = 1, \sigma_2 = 2$.

2.2.3 Contrast Equalization

The contrast equalization is the final step of the preprocessing chain. This step consists in rescaling the image intensities to standardize a robust measurement of overall contrast or intensity variation. This contrast equalization is based on the application of the following equations consecutively.

$$I_{CE}(x,y) = \frac{I(x,y)}{\left(\text{mean}\left(|I(x,y)|^{\alpha}\right)\right)^{1/\alpha}} \tag{3}$$

$$I(x,y) = \frac{I_{CE}(x,y)}{\left(\text{mean}\left(\min\left(\tau, |I(x,y)|\right)^{\alpha}\right)\right)^{1/\alpha}} \tag{4}$$

With α is a strongly compressive exponent that reduces the influence of large values; τ is a threshold used to truncate large values after the first phase of normalization.

2.3 Retina Modeling

The retina modeling is a preprocessing technique for removing illumination variation [23]. It is based on two consecutive adaptive nonlinear operations that act as an efficient light adaptation filter followed by a DoG filtering as shown in Figure 3.

For each pixel of the input image, the first nonlinear function is computed by performing a low-pass filter.

The computation of the adaptation factor $F_1(x,y)$ of each pixel is performed as follows:

$$F_1(x,y) = (I_{in}(x,y) * G_1) + \frac{\text{mean}(I_{in}(x,y))}{2} \tag{5}$$

where G_1 is a 2D Gaussian low-pass filter with standard deviation equal to 1 [23].

Using the adaptation factor F_1, the first light-adapted image $I_{la1}(x,y)$ is computed using equation (6):

$$I_{la1}(x,y) = (\max(I_{in}(x,y)) + F_1(x,y))\frac{I_{in}(x,y)}{I_{in}(x,y) + F_1(x,y)} \tag{6}$$

where $\max(I_{in}(x,y))$ is the maximum value of the image intensity.

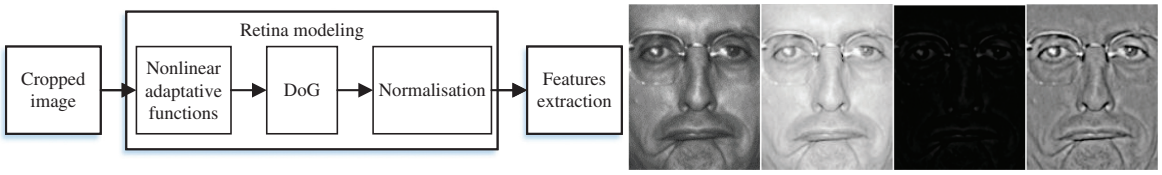

Figure 3: Retina Modeling.

The second light-adapted image $I_{la2}(x, y)$ is obtained by equation (7):

$$I_{la2}(x, y) = (I_{la1}(\max) + F_2(x, y))\frac{I_{la1}(x, y)}{I_{la1}(x, y) + F_2(x, y)} \tag{7}$$

with

$$F_2(x, y) = I_{la1}(x, y) * G_2(x, y) + \frac{\text{mean}(I_{la1}(x, y))}{2} \tag{8}$$

where G_2 is a 2D Gaussian low-pass filter with standard deviation equal to 3.

The second light-adapted image I_{la2} is then processed by DoG filter.

3 Proposed Face Recognition System

Our recognition system consists in combining two feature extraction techniques as shown in Figure 4: VLC and GOM. First, the biometric signature is verified using VLC as a feature extraction technique. If this signature is rejected, a second step is performed using GOM for feature extraction.

3.1 Vander Lugt Correlator

The VLC is one of the optical correlation techniques (OCT) that are based on the all-optical setup and are characterized by their discrimination capability and their ability of instantly detecting and estimating target objects [2, 25].

As shown in Figure 5, the VLC is composed by three planes and two lenses: the input plane, the Fourier plane, and the correlation plane. Each two planes are separated by a convergent lens. The first lens performs the Fourier transform FT of the target image. The second performs the inverse Fourier transform FT^{-1} of the multiplication result between the spectrum of the target image and the correlation filter [2].

The VLC, as shown in Figure 6, is based on the multiplication of the spectrum of the target image by a correlation filter made from a reference image. The inverse Fourier transform is then applied to the obtained image.

The similarity degree between the target and the reference images is then provided by the correlation result, which is characterized by the central correlation peak.

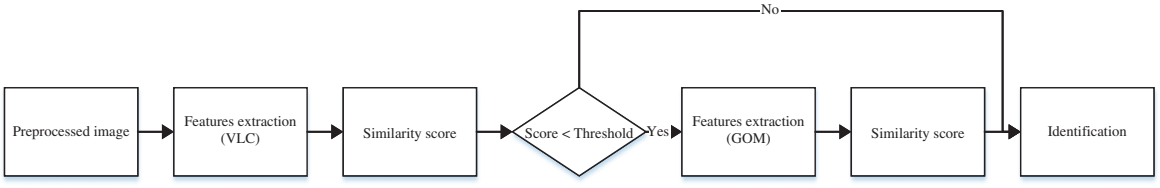

Figure 4: Proposed Face Recognition System.

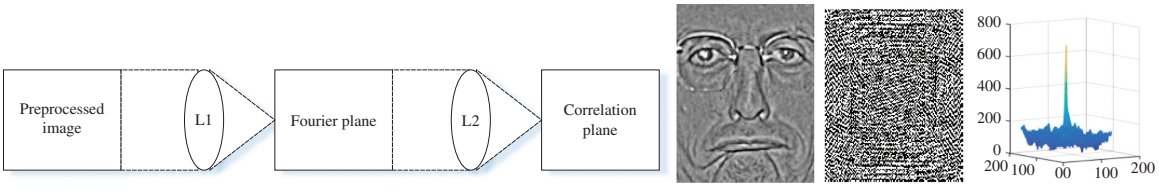

Figure 5: 4f Setup.

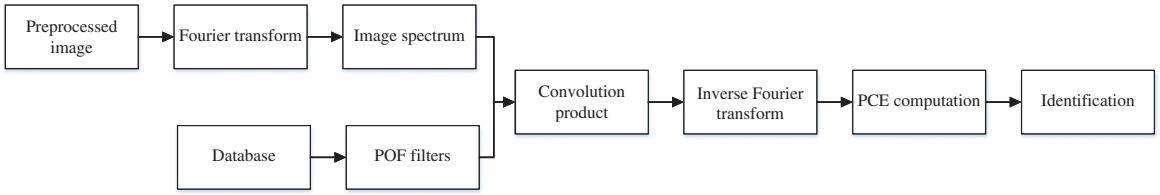

Figure 6: VLC Face Recognition System.

To evaluate the correlation, the peak-to-correlation energy (PCE) is defined by equation (9) as the energy of the peak correlation normalized to the total energy of the correlation plane.

$$\mathrm{PCE} = \frac{\sum_{i,j}^{N} E_{\mathrm{peak}}(i,j)}{\sum_{i,j}^{M} E_{\mathrm{correlation_{plane}}}(i,j)} \tag{9}$$

where N and M refer to the size of the peak correlation spot and the size of the correlation plane, respectively.

We opted for a phase-only filter: H_{POF}, where the POF is an optimized filter defined by:

$$H_{\mathrm{POF}}(\mu,\nu) = \frac{R^{*}(\mu,\nu)}{|R(\mu,\nu)|} \tag{10}$$

where $R^{*}(\mu,\nu)$ is the complex conjugate of the spectrum of the reference image.

As all optical implementations are rather complex to develop, many researchers were interested in the numerical implementation of the correlation [25], which shows a good compromise between performance and simplicity. In this work, we used the numerical implementation of VLC.

3.2 Gabor Ordinal Measures

The GOM is a local feature extraction technique that showed a good performance in pattern recognition applications due to the discrimination capability of the Gabor wavelet [15, 17] and the robustness of the ordinal measures [10, 19].

As shown in Figure 7, the process of GOM feature extraction consists mainly of five steps: 1) applying multiresolution and orientation Gabor filters to the input image, 2) deriving ordinal measures from Gabor filter responses, 3) encoding multiple ordinal measures, 4) concatenating histograms of the encoded images, and 5) applying the linear discriminant analysis to reduce the feature vector size.

3.2.1 Gabor Filters

Gabor filters are based on the Gabor wavelet [6, 7, 17], which are widely used in pattern recognition applications due to their performance that could be explained by their similarity with the visual cortex in the mammalian brain.

A family of 2D Gabor filters composed of five scales and eight orientations as shown in Figure 8 is described by equation (11) [12]:

$$\psi_{\mu,\nu} = \frac{\|k_{\mu,\nu}\|^{2}}{\sigma^{2}} e^{\left(-\frac{\|k_{\mu,\nu}\|^{2}\|z\|^{2}}{2\sigma^{2}}\right)} \left[e^{ik_{\mu,\nu}z} - e^{-\frac{\sigma^{2}}{2}}\right] \tag{11}$$

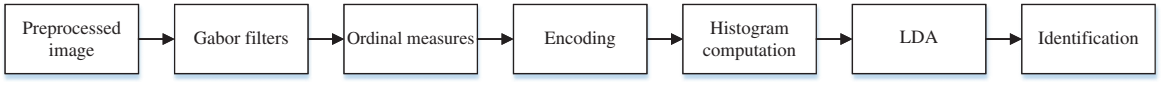

Figure 7: GOM Face Recognition System.

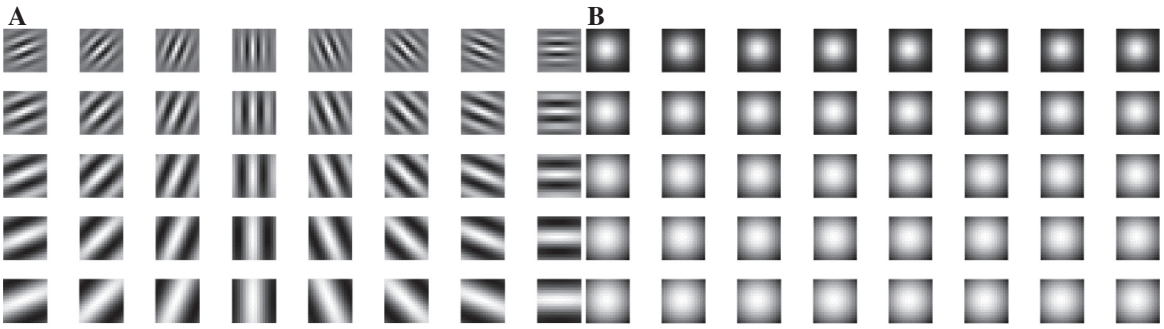

Figure 8: Gabor Wavelet Filter Bank: (A) Real Parts, (B) Magnitude.

where $\mu \in \{0, \ldots, 7\}$ and $\nu \in \{0, \ldots, 4\}$ refer to the orientations and the scales of the Gabor filters, respectively, and $z = (x, y)$ represents the spatial position. The wave vector $k_{\mu,\nu} = k_\nu e^{i\phi_\mu}$ has a magnitude $k_\nu = k_{\max}/\lambda^\nu$, where λ is the frequency ratio between filters and $\phi_\mu = \pi\mu/8$.

The response of the input image (I) to the Gabor filter family is obtained by the convolution of the image I with each filter $\psi_{\mu,\nu}$.

$$G_{\mu,\nu}(x, y) = I(x, y) * \psi_{\mu,\nu}(z) \tag{12}$$

The Gabor filtering provides four types of images: Gabor magnitude feature images, Gabor phase feature images, real Gabor feature images, and imaginary Gabor feature images.

3.2.2 Ordinal Measures

Ordinal measure is a qualitative relationship between the average intensity values of two or more image regions [19].

Ordinal measures can be defined as multi-lobe differential filters (MLDF) [4]:

$$\text{MLDF} = C_p \sum_{i=1}^{N_p} \frac{1}{\sqrt{2\pi\delta_{pi}}} e^{\left[\frac{-\left(X-\omega_{pi}\right)^2}{2\delta_{pi}{}^2}\right]} - C_N \sum_{j=1}^{N_n} \frac{1}{\sqrt{2\pi\delta_{nj}}} e^{\left[\frac{-\left(X-\omega_{nj}\right)^2}{2\delta_{nj}{}^2}\right]} \tag{13}$$

where ω and δ represent the central position and the scale of a 2D Gaussian filter, N_p and N_n are the numbers of positive and negative lobes, respectively. C_p and C_n are two constants used to maintain the balance between positive and negative lobes ($C_p N_p = C_n N_n$) as shown in Figure 9.

The ordinal features $\text{GOM\_m}^i_{\mu,\nu}$, $\text{GOM\_p}^i_{\mu,\nu}$, $\text{GOM\_r}^i_{\mu,\nu}$ and $\text{GOM\_i}^i_{\mu,\nu}$ are extracted as follows:

For Gabor magnitude feature images $M_{\mu,\nu}$:

$$\text{GOM\_m}^i_{\mu,\nu}(x, y) = \begin{cases} 1 & \text{if } M_{\mu,\nu}(x, y) * \text{MLDF}^i > 0 \\ 0 & \text{if } M_{\mu,\nu}(x, y) * \text{MLDF}^i \leqslant 0 \end{cases} \tag{14}$$

For Gabor phase features image $\theta_{\mu,\nu}$:

$$\text{GOM\_p}^i_{\mu,\nu}(x, y) = \begin{cases} 1 & \text{if } 0 \leqslant \left|\theta_{\mu,\nu}(x, y) * \text{MLDF}^i\right| \leqslant 0.5\pi \\ 0 & \text{if } 0.5\pi < \left|\theta_{\mu,\nu}(x, y) * \text{MLDF}^i\right| \leqslant 2\pi \end{cases} \tag{15}$$

For real Gabor features image $Re_{\mu,\nu}$:

$$\text{GOM\_r}^i_{\mu,\nu}(x, y) = \begin{cases} 1 & \text{if } Re_{\mu,\nu}(x, y) > 0 \\ 0 & \text{if } Re_{\mu,\nu}(x, y) \leqslant 0 \end{cases} \tag{16}$$

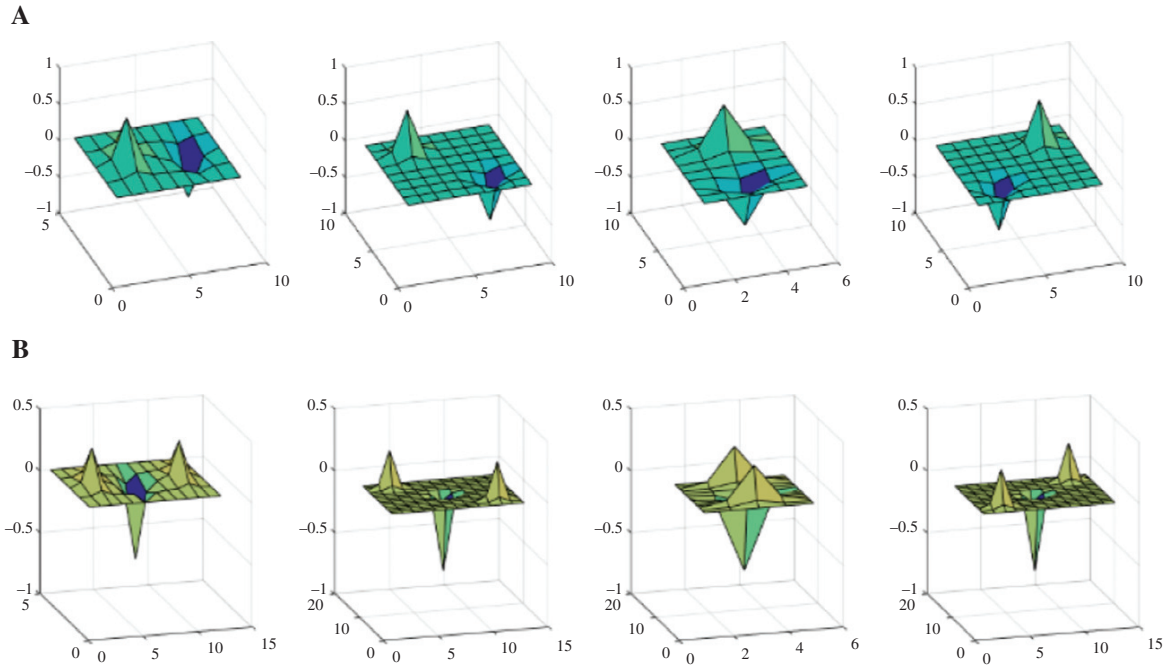

Figure 9: Ordinal Filters: (A) Bi-Lobe, (B) Tri-Lobe.

For imaginary Gabor features image $Im_{\mu,v}$:

$$\text{GOM\_i}^{i}_{\mu,v}(x,y) = \begin{cases} 1 & \text{if } Im_{\mu,v}(x,y) > 0 \\ 0 & \text{if } Im_{\mu,v}(x,y) \leqslant 0 \end{cases} \tag{17}$$

with $i \in \{1, \ldots, 8\}$

3.2.3 Encoding *GOM_α* Features

The **GOM**_$\alpha^{i}_{\mu,v}$ feature obtained from the i^{th} ordinal filter is a binary image. As we used eight orientations, the eight resultant binary images can be combined to form a grayscale image **GOM_map**_α^{i}_{v} for each scale v (as shown in Figure 10).

The encoding is described by equation (18):

$$\text{GOM\_map\_}\alpha^{i}_{v}(x,y) = \sum_{\mu=0}^{7}\left(\text{GOM\_}\alpha^{i}_{\mu,v}(x,y) * 2^{\mu}\right) \tag{18}$$

where $\alpha \in$ {m: magnitude, p: phase, r: real, i: imaginary} and GOM_map_$\alpha^{i}_{v}(x,y)$ is the texture primitive obtained at (x,y) for the i^{th} ordinal measure at scale v.

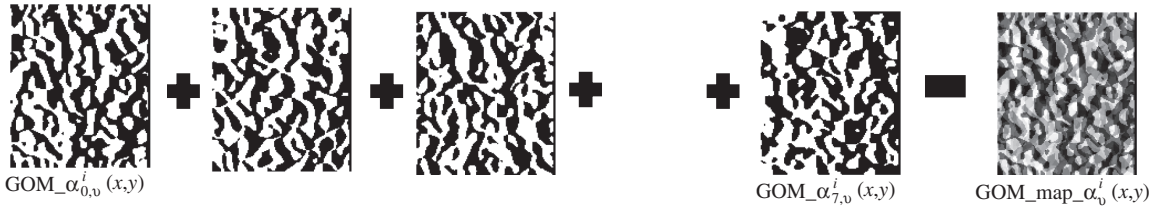

Figure 10: GOM Encoding Process.

3.2.4 Histogram Representation

The obtained **GOM_map**_α are divided into blocks. For each block, a 64-bin histogram is calculated, followed by L2hys normalization. Normalized histograms of the different **GOM_map** are concatenated to form a GOM feature.

3.2.5 Linear Discriminant Analysis (LDA)

The LDA is a statistical approach widely used in dimensionality reduction and supervised classification to find the set of projection vectors, which maximize the between-class and minimize the within-class. This technique is used to reduce the feature vector dimension of each block.

4 Experiments

4.1 FERET Database

The performance of the proposed technique is evaluated using the FERET database [14], which is one of the most used databases in face recognition research community. It contains standard partitions: a gallery (Fa) and two probe sets (Fb) and (Fc), where the gallery (Fa) contains 1196 frontal face images as shown in Figure 11 with one image per person, the (Fb) probe set contains 1195 images with different facial expressions, and the (Fc) probe set contains 194 images with variations of lighting.

To evaluate our system, we used the gallery for the identification stage and the training set, which contains 1002 images for 429 subjects, for the LDA.

4.2 Extended YaleB Database

This database contains frontal face images under various illumination and expression conditions for 38 persons. In total, it has 2412 images. We used one image per person for the training and the rest for the evaluation [13].

4.3 Experimental Settings

A preprocessing step is performed before the evaluation of the different algorithms. A geometrical normalization of the images consists in resizing the image to a 128×160 region of interest according to the position of the eyes. In order to reduce the effect of the illumination variation, local shadowing, and highlights, the two preprocessing sequences proposed by Tan and Triggs [20] and Son Vu and Caplier [23] are performed.

For the proposed recognition system, as shown in Table 1, we performed eight tests with the two preprocessing techniques. For the first four tests, we used only one feature extraction technique.

In the first and second tests, we, respectively, performed Tan and Triggs and retina modeling as a preprocessing method and VLC for feature extraction.

Figure 11: Examples of FERET Database Images.

Table 1: Test Scenarios.

	Preprocessing technique	Feature extraction
Test 1	Tan and Triggs	VLC
Test 2	Retina modeling	VLC
Test 3	Tan and Triggs	GOM
Test 4	Retina modeling	GOM
Test 5	Tan and Triggs	VLC and GOM
Test 6	Retina modeling	VLC and GOM
Test 7	Retina modeling	VLC
	Tan and Triggs	GOM
Test 8	Tan and Triggs	VLC
	Retina modeling	GOM

In the third and fourth tests, we, respectively, performed Tan and Triggs and retina modeling as a preprocessing method and GOM for feature extraction.

For the fifth, sixth, seventh, and eighth tests, we combined the two feature extraction techniques.

For the fifth test, we first performed the Tan and Triggs test for both VLC and GOM.

For the sixth test, we first performed the retina modeling for both VLC and GOM.

For the seventh test, we performed the retina modeling for the VLC and Tan and Triggs for the GOM.

Finally, we performed Tan and Triggs for the VLC and the retina modeling for the GOM.

In the GOM method, we used only the Gabor magnitude features. We reduced the dimension of each block feature vector from 2560 to 260 using LDA. The cosine distance is then used for the classification.

4.4 Results and Discussion

From test 1 and test 2 in Table 2, we can see that the VLC technique gives better results when using Tan and Triggs techniques. This can be explained by the fact that the spectrum of the preprocessed image using the Tan and Triggs method is richer than the retina modeling as shown in Figure 12.

Table 2: FERET Data Sets Result.

	Enhancement techniques	Feature extraction	Fb	Fc
Test 1	Tan and Triggs	VLC	77.41	85.57
Test 2	Retina modeling	VLC	73.72	81.96
Test 3	Tan and Triggs	GOM	98.16	99.48
Test 4	Retina modeling	GOM	99.00	99.48
Test 5	Tan and Triggs	VLC and GOM	98.16	99.48
Test 6	Retina modeling	VLC and GOM	99.00	99.48
Test 7	Tan and Triggs	VLC	99.00	99.48
	Retina modeling	GOM		
Test 8	Retina modeling	VLC	98.16	99.48
	Tan and Triggs	GOM		

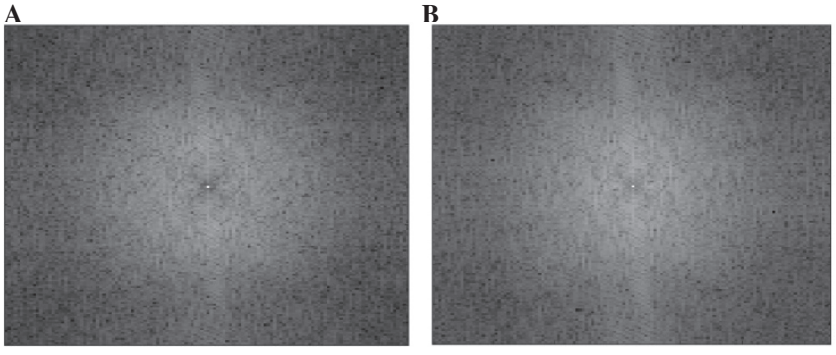

Figure 12: Image Spectrum Using (A) Tan and Triggs, (B) Retina Modeling.

However, the retina processing contains a low-pass filtering step, which eliminates high frequencies containing information useful for the recognition.

From tests 3 and 4 in Table 2, we deduce that for the GOM feature extraction, the two preprocessing techniques give almost the same results for Fb and Fc.

From the last four tests (test 5 to test 8), in which we combined the two feature extraction techniques VLC and GOM, we deduce that test 7 gives a better recognition rate when using, respectively, Tan and Triggs and retina modeling for image enhancement.

Table 3 shows the mean computation time for each data set using the proposed system. This time is computed as follows:

$$Tm = \frac{WC_{\mathrm{VLC}} * T_{\mathrm{VLC}} + MC_{\mathrm{VLC}} * T_{\mathrm{GOM}}}{WC_{\mathrm{VLC}} + MC_{\mathrm{VLC}}} \tag{19}$$

where WCVLC is the number of well-classified images using VLC, TVLC is the mean computational time of VLC, MCVLC is the number of misclassified images using VLC, and TGOM is the mean computational time of GOM.

Figure 13 shows that the proposed system based on the combination of VLC and GOM almost outperforms the GOM algorithm on each probe set.

Table 3: Mean Computation Time per Image.

Data set	Proposed method (ms)	GOM (ms)
Fb	107	486
Fc	69	486

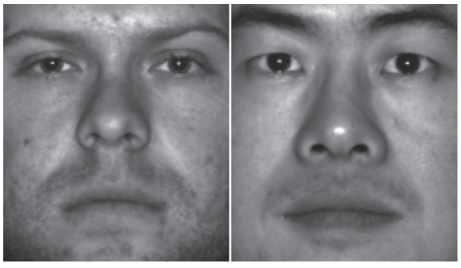

Figure 13: Examples of Extended YaleB Database Images.

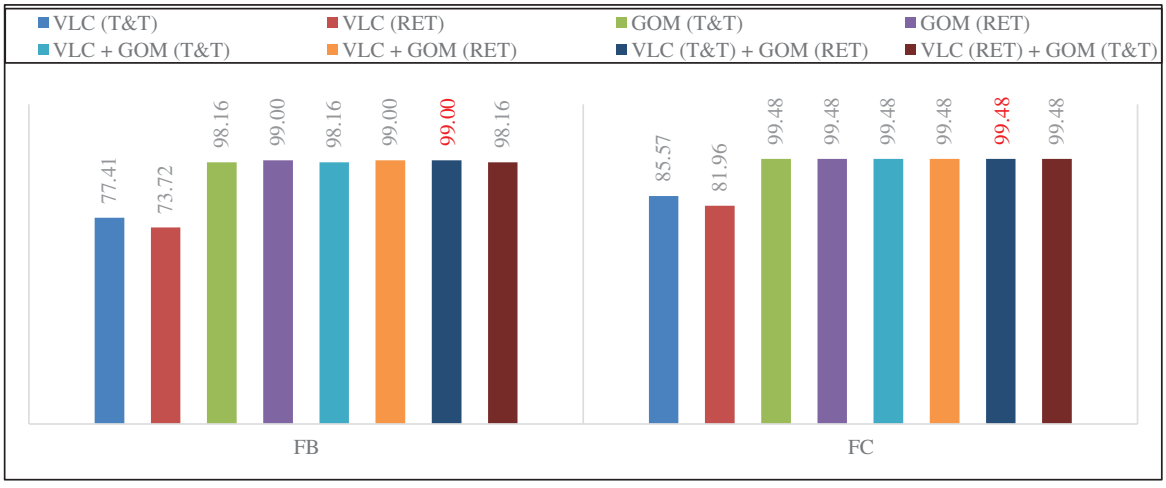

Figure 14: Results on Each Probe Set of FERET.

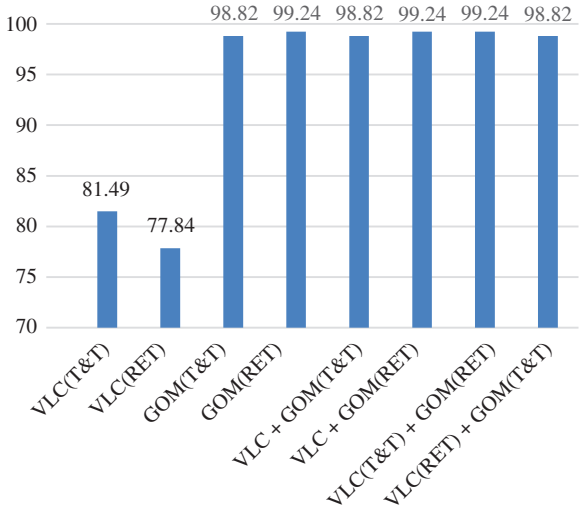

Figure 15: Results on the Whole FERET Database.

Table 4: Results on Extended YaleB Database.

Method	Recognition rate (%)
ADL + SVM [16]	82.91
SRC [24]	80.5
LC-KSVD [11]	95
SADL [22]	94.91
VLC + GOM	96.21

Figure 14 shows that the proposed system based on the combination of VLC and GOM almost outperforms the GOM algorithm on the whole FERET database (see Figure 15).

Table 4 shows the recognition rate of the proposed technique on the extended YaleB database using one image for the training and the rest for the testing. This table shows that our system outperforms other systems, although we only used one image for the training stage.

5 Conclusion

We combined the VLC and GOM feature extraction techniques in order to reduce the computational time and improve the accuracy of our face recognition system. Before each extraction technique, a preprocessing step was performed. We processed eight test scenarios to compare the effect of the preprocessing techniques on the performance of our system.

The results clearly showed that combining Tan and Triggs with the VLC and retina modeling with the GOM outperformed the other combinations on all the probe sets of the FERET database.

In this work, we proposed a new face recognition system that combines the VLC and GOM as feature extractions. This system outperforms systems based on the GOM technique in recognition rate and computation time.

Despite combining the GOM and VLC, the computation time for the system was still important due to the use of the Gabor wavelet. Our next work shall consist in a face recognition system that maintains the recognition rate performed by GOM and VLC and reduce the computation time.

Bibliography

[1] A. Alfalou and C. Brosseau, Understanding correlation techniques for face recognition: from basics to applications, in: Oravec, M. (ed.), *Face Recognition*, IntechOpen, Rijeka, Croatia, 2010. doi: 10.5772/8935. Available from:

https://www.intechopen.com/books/face-recognition/understanding-correlation-techniques-for-face-recognition-from-basics-to-applications.
[2] A. Blake and M. Isard, Active shape models. In: *Active Contours*. Springer, London, 1998.
[3] X. Cao, Y. Wei, F. Wen and J. Sun, Face alignment by explicit shape regression, *Int. J. Comput. Vis.* **107** (2013), 177–190.
[4] Z. Chai, Z. Sun, H. Mendez-Vazquez, R. He and T. Tan, Gabor ordinal measures for face recognition, *IEEE Trans. Inf. Foren. Sec.* **9** (2014), 14–26.
[5] T. Cootes, G. Edwards and C. Taylor, Active appearance models, *IEEE Trans. Pattern Anal. Mach. Intell.* **23** (2001), 681–685.
[6] J. Daugman, Two-dimensional spectral analysis of cortical receptive field profiles, *Vis. Res.* **20** (1980), 847–856.
[7] J. Daugman, Uncertainty relation for resolution in space, spatial frequency, and orientation optimized by two-dimensional visual cortical filters, *J. Opt. Soc. Am A* **2** (1985), 1160.
[8] M. Elbouz, F. Bouzidi, A. Alfalou, C. Brosseau, I. Leonard and B. Benkelfat, Adapted all-numerical correlator for face recognition applications, *Opt. l Pattern Recognit.* **XXIV** (2013), 874807-1–874807-8.
[9] A. Ghorbel, I. Tajouri, W. Aydi and N. Masmoudi, A comparative study of GOM, uLBP, VLC and fractional Eigenfaces for face recognition, in: *2016 International Image Processing, Applications And Systems (IPAS)*, pp. 1–5, IEEE, Hammamet, Tunisia, 2016.
[10] R. He, T. Tan, L. Davis and Z. Sun, Learning structured ordinal measures for video based face recognition, *Pattern Recognit.* **75** (2018), 4–14.
[11] Z. Jiang, Z. Lin and L. Davis, Label Consistent K-SVD: learning a discriminative dictionary for recognition, *IEEE Trans. Pattern Anal. Mach. Intell.* **35** (2013), 2651–2664.
[12] M. Lades, J. Vorbruggen, J. Buhmann, J. Lange, C. von der Malsburg, R. Wurtz and W. Konen, Distortion invariant object recognition in the dynamic link architecture, *IEEE Trans. Comput.* **42** (1993), 300–311.
[13] K. Lee, J. Ho and D. Kriegman, Acquiring linear subspaces for face recognition under variable lighting, *IEEE Trans. Pattern Anal. Mach. Intell.* **27** (2005), 684–698.
[14] P. Phillips, H. Moon, S. Rizvi and P. Rauss, The FERET evaluation methodology for face-recognition algorithms, *IEEE Trans. Pattern Anal. Mach. Intell.* **22** (2000), 1090–1104.
[15] Á. Serrano, I. de Diego C. Conde and E. Cabello, Recent advances in face biometrics with Gabor wavelets: a review, *Pattern Recognit. Lett.* **31** (2010), 372–381.
[16] S. Shekhar, V. M. Patel and R. Chellappa, Analysis sparse coding models for image-based classification, in: *2014 IEEE International Conference on Image Processing (ICIP)*, pp. 5207–5211, IEEE, 2014. doi: 10.1109/icip.2014.7026054.
[17] L. Shen and L. Bai, A review on Gabor wavelets for face recognition, *Pattern Anal. App.* **9** (2006), 273–292.
[18] Y. Sun, X. Wang and X. Tang, Deep convolutional network cascade for facial point detection, in: *Proceedings of the IEEE Conference on Computer Vision and Pattern Recognition*, pp. 3476–3483, IEEE, Portland, OR, 2013.
[19] T. Tan and Z. Sun, Ordinal representations for biometrics recognition, in: *15th European Signal Processing Conference*, IEEE, Paris, France, 2007.
[20] X. Tan and B. Triggs, Fusing Gabor and LBP feature sets for kernel-based face recognition, in: *International Workshop on Analysis and Modeling of Faces and Gestures*, pp. 235–249, Springer, Berlin, Heidelberg, 2007.
[21] X. Tan and B. Triggs, Enhanced local texture feature sets for face recognition under difficult lighting conditions, *IEEE Trans. Image Process.* **19** (2010), 1635–1650.
[22] W. Tang, A. Panahi, H. Krim and L. Dai, Structured analysis dictionary learning for image classification (2018). http://arxiv.org/1805.00597.
[23] N.-S. Vu and A. Caplier, Illumination-robust face recognition using retina modeling, in: *2009 16th IEEE International Conference on Image Processing (ICIP)*, pp. 3289–3292, IEEE, Cairo, Egypt, 2009.
[24] J. Wright, A. Yang, A. Ganesh, S. Sastry and Y. Ma, Robust face recognition via sparse representation, *IEEE Trans. Pattern Anal. Mach. Intell.* **31** (2009), 210–227.
[25] E. Zhou, H. Fan, Z. Cao, Y. Jiang and Q. Yin, Extensive facial landmark localization with coarse-to-fine convolutional network cascade, in: *Proceedings of the IEEE International Conference on Computer Vision Workshops*, pp. 386–391, IEEE, Sydney, NSW, 2013.